Modelling of stylolite geometries and stress scaling

[a]Koehn, D., [b]Ebner, M., [c]Renard, F., [d]Toussaint, R., [e]Passchier, C.W.

[a] School of Geographical and Earth Sciences, University of Glasgow, Gregory building, Lilybank Gardens, Glasgow G12 8QQ, UK
[b] Geological Survey of Austria, Neulinggasse 38, A1030 Vienna, Austria
[c] CNRS-Observatoire, Université Joseph Fourier BP 53, F-38041 Grenoble, France & Physics of Geological Processes, University of Oslo, Norway
[d] Institut de Physique du Globe de Strasbourg (IPGS), CNRS and University of Strasbourg (EOST), 5 rue Descartes, F-67084 Strasbourg Cedex, France
[e] Tectonophysics, Institute of Geosciences, Johannes Gutenberg University, Becherweg 21, 55099 Mainz, Germany

Abstract

In this contribution we present numerical simulations of stylolite growth to decipher the effects of initial rock heterogeneity and stress on their morphology. We show that stylolite growth in a rock with a uniform grain size produces different patterns than stylolite growth in a rock with a bimodal grain size distribution. Strong pinning of large heterogeneities produce stylolite structures that are dominated by pronounced teeth, whereas a uniform grain size leads to spikes and a roughness that shows variable wavelengths. We compare the simulated stylolites with natural examples and show that the model can reproduce the real structures. In addition we show that strong pinning in the bimodal case can lead to a linear stylolite roughness growth in contrast to the non-linear growth of stylolites that develop from a uniform noise. In a set of 24 simulations we vary the main principle stress on the stylolite in order to test if our model can reproduce the analytically derived stress-scaling proposed by Schmittbuhl et al. (2004). We compare the calculated stresses with the applied stresses and show that the numerical model and the analytical solution are in good agreement. Our results strengthen the hypothesis that stylolites can be used as strain and stress gauges to estimate not only the orientation of paleo-stresses, but also their absolute values of formation stresses and amounts of compaction.

Keywords: stylolite, stress-gauge, compaction, pressure solution, numerical model, self-affinity

1. Introduction

Pressure solution is an important deformation mechanism that takes place in the upper parts of the Earth's crust (Rutter, 1983). This mechanism of dissolution, transport and precipitation of material starts as shallow as 90m during diagenesis in sedimentary basins (Tada & Siever 1989) and may still be active during high grade metamorphic conditions (Beach, 1979). If the dissolution of material takes place in a localized manner, rough dissolution surfaces develop that are termed stylolites (Fig. 1, Dunnington, 1954; Heald, 1955; Park & Schot, 1968; Guzzetta, 1984; Merino, 1992; Railsback, 1993; Karcz & Scholz, 2003). Stylolites are very common in a variety of mono-mineralic rock types and have several distinct characteristics: they concentrate material that cannot be dissolved as fast as the matrix appearing as dark seams, the surface has a pronounced roughness of peaks or spikes with parallel or inward sloping sides, such that they can be pulled apart without breaking the rock; and this roughness occurs on a range of scales (Fig. 1).

Geologists are interested in stylolites because they are used to estimate the compaction and the stress history in sedimentary basins (Ebner et al. 2009b, Petit & Mattauer 1995, Rispoli 1981). The hydrocarbon industry is mainly interested in stylolites because they affect reservoir properties; they can be sealing because of their clay content and reduce porosity and permeability around the stylolite, while they may also act as channel-ways when fluids travel along the stylolite interface (Fabricius & Borre, 2007; Baron & Parnell, 2007). The use of stylolites to estimate compaction and stress is of great interest to Earth scientists and may be used for basin analysis or tectonic studies in fold and thrust belts. Reliable paleo-stress gauges are rare in geology. For several reasons we are convinced that stylolites can play this role: (1) Stylolites are very common geological structures and (2) the orientation of their teeth track

the direction of the main compressive stress, (3) the magnitude of these asperities capture part of the compaction history of the host-rock and (4) it has been demonstrated that the stylolite roughness can be used to estimate absolute stress values, i.e. the mean, differential and the principal stress values (Ebner et al., 2009b, 2010a). A few other paleo-stress markers exist, as e.g. the study of calcite twins in rocks (Burkhard. 1993, Lacombe, 2010), but they are generally more sensitive to the stress orientation than to its magnitude. It is useful to develop additional paleo-stress gauges, which can be applied on a variety of rocks, such as stylolites that are present in many sedimentary rocks.

2. The use of stylolites for structural analysis

Stylolite morphology develops according to two main processes. Firstly, an interface can either be initially present in the sediment, such as the interface between two different sedimentary layers or a fracture, or they form by propagation from an initial site of stress concentration that promotes the formation of an anticrack (Fletcher and Pollard, 1981), localize due to chemical effects induced by micas (Aharonov and Katsman 2009) or localized volume reduction (Katsman et al. 2006). Secondly, such interface may roughen with time, a process that is dependent on local stress conditions and the amount of heterogeneities in the rock. Stylolites can be used in structural analysis to find three parameters: the main compressive stress direction (e.g. Rispoli, 1981, Koehn et al. 2007), the amount of compaction and the product of the differential and mean stress (Ebner et al, 2009b, Ebner et al. 2010a). Stylolite teeth (Fig. 2a) are thought to grow parallel to the main compressive stress direction, a hypothesis that was strengthened by recent numerical simulations (Ebner et al. 2009a, Koehn et al. 2007). These simulations show that the lateral position of a tooth along a stylolite interface is random but its shape is strongly deterministic with respect to the orientation of the direction of maximum finite compaction, which is identical with the main compressive stress orientation in homogeneous solids. The amplitude of a stylolite can be

used indirectly to calculate the amount of compaction. Although this can be difficult, the non-linear scaling relationship between finite compaction and average stylolite amplitude gives reasonable estimates (Koehn et al. 2007). Without the use of a scaling function one can estimate the amount of dissolved material at the stylolite by using its maximum height, but this requires the observation of this maximum in a few spots, which can be hidden in the rock in some situations. Hence, the maximum height observed corresponds to a lower bound of the dissolution (amount of compaction along the stylolite) that took place, and not necessarily the total one. The scaling function given by Koehn et al. (2007) can be used to estimate compaction; however the function is non-linear leading to a relatively large uncertainty in the result.

The third and most important value that can be determined from natural stylolites is the product of the differential and mean stress, which can be calculated from the scaling of the stylolite roughness (Renard et al., 2004), based on an analytical solution presented in Schmittbuhl et al. (2004). This analytical solution demonstrates that the stresses acting during stylolite formation can be derived from the stylolite roughness hidden in the crossover-length scale that separates two self-affine scaling regimes well documented for natural stylolites. Ebner et al. (2009b) showed in a study on natural bedding parallel stylolites, which were sampled at different depths in a sedimentary basin, that the measured principal normal stress value increases linearly with the depth of stylolite formation, which supports the analytical solution. These authors also present a method that allows the calculation of the full paleo-stress tensor from the stylolites under favourable conditions. In addition Ebner et al. (2010a) show with a study on tectonic stylolites that these can reveal the difference between all three principal stress components, which is an additional support for the theory of Schmittbuhl et al. (2004).

In order to further test the hypothetical scaling relation of the stylolite roughness as a function to overburden stress, we present two-dimensional numerical simulations of the roughness

development of a set of sedimentary stylolites and their sensitivity to stress. First we present different stylolite geometries that develop in a limestone with a constant grain size versus a limestone with a bimodal distribution of grains (or fossils). Then we test the analytical solution of Schmittbuhl et al. (2004) and show with a numerical model (Koehn et al., 2007) how stylolites can be used to attain the full paleo-stress tensor and the paleo-depth of (bedding parallel) stylolite growth in a sedimentary basin. In addition we validate our numerical simulations by showing that they result in stylolite geometries found in nature and we show that the model reproduces the crossover length scale that is predicted by the solution of Schmittbuhl et al. (2004) for a given stress.

3. The stress gauge

Detailed measurements of stylolite roughness (Renard et al. 2004, Ebner et al. 2009b), as well as deterministic models of stylolite formation (Schmittbuhl et al. 2004, Koehn et al. 2007) indicate that the absolute value of the stress can be determined from the roughness of a stylolite. Stylolites are thought to roughen because of the existence of heterogeneities in a rock that dissolve at different rates than the host-rock. In limestone, these heterogeneities may be fossils on a millimetre scale or clay particles, oxide or quartz grains on a micrometer scale. Impurities are localizing dissolution and in some cases enable stylolite formation (Aharonov and Katsman, 2009) and collect within the stylolite surface during successive stress driven dissolution of the host-rock. The host-rock dissolves on both sides of the stylolite. If this dissolution is locally heterogeneous, so that one part of the host-rock on one side of the stylolite dissolves slower than the other, the interface starts to become rough (Fig. 2a,b). In an extreme case an impurity like an oxide grain can pin one side of the stylolite host-rock completely, so that this side does not dissolve at all. The pinning particle is then quasi pushed into the host-rock on the other side of the stylolite and a spike develops. For example, Ebner

et al. (2010b) have shown with an EBSD analysis that small quartz grains pin corners of some stylolite teeth (Fig. 2c).

The developing stylolite roughness can be accurately described by a self-affine scaling function with a characteristic Hurst or roughness exponent (Brouste et al. 2007, Gratier et al. 2005, Renard et al. 2004, Schmittbuhl et al. 2004). When a rough surface shows a self-affine property, its roughness has a variable amplitude (A) over wavelength (λ) ratio at different scales. A self-affine 1D profile can be described mathematically as invariant under self affine transformations, i.e. anisotropic zooms of any pair of factors (b, b^{α}), where b is real, respectively for the sub-parallel and normal direction to the average surface: A zoom transformation on the surface in the x-direction by $x \rightarrow bx$ and in height by $h \rightarrow b^{\alpha} h$, where x is oriented parallel to the stylolite interface, h is the height of the interface, b is a linear scaling factor and α the Hurst or roughness exponent (Barabasi & Stanley 1995). If the roughness exponent is smaller than 1.0 the profile is called self-affine: it appears flat on the large scale and rougher (with larger aspect ratio A/λ of out of plane amplitude over in plane wavelength) on the small scale. Such a scaling is reproduced by the natural stylolite shown in Figure 1, where the stylolite seems flat on the larger scale (Fig. 1a, width 40cm, low ratio A/λ) and appears progressively rougher on the small scale (Fig. 1c,d, width 6cm and 4mm, higher ratio A/λ). Natural stylolites tend to show not only one but two characteristic roughness exponents. On the large scale the exponent is around 0.5 whereas on the small scale it is close to 1 (Renard et al., 2004, Schmittbuhl et al. 2004). The change from one scaling regime to the other (characterized by different scaling exponents) is relatively sharp. It lies typically on the millimetre length scale and is termed crossover-length *(l)*. An interface with a roughness exponent of about 1.0 is called self-similar, and does not change its roughness aspect ratio A/λ with different scales, which can also be seen in Figure 1c,d, where the amplitude over wavelength ratio does not change significantly (width 4mm and 0.8mm).

159 Schmittbuhl et al. (2004) could show with their analytical solution that these two roughness
160 exponents correspond to two different thermodynamic regimes where surface energy is
161 dominant on the small scale and elastic energy dominant on the large scale, with a well-
162 defined cross-over length at the millimetre scale.
163 It is important to notice that surface and elastic energies tend to flatten the interface whereas
164 the heterogeneities initially present in the host rock i.e. a quenched noise roughen the
165 interface (Koehn et al. 2007, Schmittbuhl et al. 2004). The surface energy in the rock stays
166 constant whereas the elastic energy is a function of the stress field surrounding the stylolite.
167 When the stress increases because the stylolite grows for example in deeper parts of a
168 sedimentary basin the elastic energy also increases and the cross-over between surface and
169 elastic energy dominated regimes shifts to smaller scales. Hence the influence of surface
170 energies is shifted to smaller scales with increasing stress. Determining the cross-over from
171 natural stylolites thus gives a value for the stress on the stylolite interface. The scaling
172 relation from Schmittbuhl et al. (2004) relates the cross-over length scale *(l)* with the product
173 of the mean (σ_m) and differential (σ_{dif}) stress according to

174 $$l = \frac{\gamma E}{\beta} \frac{1}{\sigma_m \sigma_{dif}}, \qquad (1)$$

175 where γ is the surface free energy, E the Young's modulus and β a function of the Poisson
176 ratio ($\beta = \nu(1-2\nu)/\pi$). In a sedimentary basin with a uniaxial vertical stress component (i.e.
177 zero horizontal displacements) and the horizontal components being a function of the vertical
178 stress component σ_z, equation (1) simplifies to (modified after Ebner et al. 2009b)

179 $$l = \frac{\gamma E}{\kappa} \frac{1}{\sigma_z^2}, \qquad (2)$$

180 where κ is a function of the Poisson ratio ($\kappa = \frac{\nu}{3\pi} \frac{(1-2\nu)^2(1+\nu)}{(1-\nu)^2}$). This scaling relation is
181 only valid for bedding parallel stylolites (sedimentary stylolites), for which the principal

182 horizontal stresses are equal if one assumes no lateral displacement. For tectonic stylolites
183 with 3 different main compressive stresses this solution cannot be applied since in that case
184 the differential stresses vary. An approximation for the complex tectonic case is given in
185 Ebner et al. (2010a). In the present contribution we want to test the scaling relation for
186 sedimentary stylolites with the numerical simulations of Koehn et al. (2007) and illustrate
187 how the stylolite morphology varies with increasing depth in a sedimentary basin. This
188 comparison between natural data (Ebner et al., 2009b), an analytical model (Schmittbuhl et
189 al., 2004) and numerical simulations will allow us to propose that stylolites can be used as
190 stress gauges.
191
192 **4. Numerical model**
193 We use the numerical model of Koehn et al. (2003, 2006, 2007), Bons et al. (2008) and
194 (Ebner et al. 2009a). It is based on a 2D linear elastic lattice spring model where elements can
195 dissolve as a function of surface energy, elastic energy and normal stress at the interface.
196 Dissolution takes place at a predefined surface that is initially smooth (Fig. 3). Particles on the
197 interface are stressed when they are in contact. We calculate the surface energy at the
198 interface and the elastic energy of the particle (Koehn et al., 2007) and use these in addition to
199 the difference between the normal stress at the particle surface and the average normal stress
200 across all particles at the interface to determine how fast the particle dissolves according to
201 (Koehn et al., 2007)
202 $$D_i = k_i V_s \left(1 - \exp\left(\frac{-\Delta\sigma_n V_s - \Delta\psi}{RT}\right)\right), \qquad (3)$$
203 where D_i is the dissolution rate of particle i, k_i a rate constant, V_s the molecular volume, $\Delta\sigma_n$
204 the difference in normal stress along the interface, $\Delta\Psi_s$ the difference in Helmholtz free
205 energy of the solid (the sum of elastic and surface energies at a particle) between a curved
206 stressed interface and a flat unstressed interface, R the universal gas constant and T the

absolute temperature (in Kelvins). Note that we are using the difference in normal stress between the average normal stress on all interface particles and the particle's normal stress. We are not using the stress difference between an unstressed surface and a stressed surface. If we use the difference between an unstressed and a stressed surface the normal stress term is too dominant and the crossover does not appear in the simulations. We assume that the structure is constantly dissolving so that diffusion and precipitation of material are not taken into account. However, since we use the normal stress difference between the average stress and the local stress we model a situation where the fluid has a concentration of dissolved material that is proportional to the average normal stress on the stylolite.

Roughening of the surface is induced by randomly oriented slower dissolving particles (5%) that pin the interface until they themselves dissolve (Fig. 3a). In the case of a bimodal grain size we include slower dissolving larger grains (or fossils), defined by clusters of particles. These clusters themselves contain a noise on a smaller scale, so that they contain particles that dissolve slower than the cluster itself (Fig. 3b). For the presented simulations the numerical model has two resolutions, the smaller resolution of 184000 particles, a real physical width of 4cm and a particle size of 0.1 mm is used for simulations that have a noise and grain size on one scale whereas a larger resolution of 736000 particles and a real physical width of 8cm is used for simulations with a bimodal distribution of noise and grain size. Additional parameters are a Poisson ratio of 0.33 (determined by the shape of lattice used), a Youngs modulus of 80 GPa and a surface free energy of 0.27 J/m^2 relevant for limestone. The molar volume for calcite is 0.00004 m^3/mol, the temperature is 300K and the dissolution constant for calcite is 0.0001 $mol/(m^2s)$ (Clark, 1966; Renard et al., 2004; Schmittbuhl et al., 2004; Koehn et al., 2007). The deformation is uniaxial with fixed side-walls simulating stylolite formation in a sedimentary basin, the vertical stress is constant for the simulation with a bimodal noise (50 MPa) and is varied between 29 and 92 MPa (29, 41, 50, 57, 64, 71, 80, 92) for simulations with a noise that is only on the particle scale.

5. Results of the simulations

5.1. Comparison of natural and simulated stylolites

We use two different initial setups for the simulations, which are illustrated in figure 3. In the first setup we use a random distribution of slower dissolving particles in the model, these are shown as dark particles in figure 3a. In all these simulations 5% of particles dissolve 20% slower than the rest. This means that they can pin the surface, but they may dissolve themselves if elastic or surface energies at the tips of spikes become too large or if two slower dissolving particles meet at the interface (Koehn et al., 2007). In the second set of simulations we add larger grains (also 5%) that dissolve 20% slower (fig. 3b); they are defined as clusters of particles. These larger grains are added on top of the initial distribution of slower dissolving particles. This means that the slower dissolving grains also contain particles that dissolve slower and the noise is bimodal.

The developing geometries are shown in figure 4 where we compare the simulated patterns with natural examples. Figure 4a shows a stylolite that was simulated when using a bimodal noise. The larger grains at the interface are shown in grey. The stylolite geometry clearly reflects the bimodal nature of the noise. The largest grains pin the interface and result in extreme teeth with very straight edges. The stylolite surface between the large grains shows much smaller roughness amplitude, that slowly develops into larger wavelengths. This surface is on average still in the middle of the stylolite and resembles the orientation of the initially flat interface where dissolution started. The teeth that are pinned by larger grains have variable height depending on when the pinning grains (clusters of slower dissolving particles in our model setup) meet the interface. The surface on top or at the bottom of the teeth shows a roughness that is similar to the normal stylolite roughness indicating that the pinning grains slowly dissolve themselves. The actual dissolution of the host-rock is indicated by the grey bar on the right hand side of the simulated stylolite. One can observe that the distance

between the highest and lowest teeth on each side of the stylolite almost reflects the actual dissolution. Large grains started to pin the interface relatively early and are not yet completely dissolved so that the actual dissolution is still recorded by the stylolite. The picture on the right hand side shows a stylolite from the "Muschelkalk" limestone of southern Germany where large fossils pin the interface resulting in large teeth. The noise is clearly bimodal and the simulation captures the geometries of the real stylolite.

Figure 4b shows a simulation with a noise only on the particles and a similar natural stylolite on the right hand side. The simulated stylolite shows the typical geometry that was discussed in Koehn et al. (2007) and Ebner et al. (2009) with the development of variable wavelengths and amplitudes of roughness. Extreme spikes can develop if single particles pin the interface for a long time, meaning that they probably meet no slowly dissolving particle on the other side of the interface. The spikes are not as straight as the teeth that develop when the noise is bimodal (Fig. 4a). The grey bar on the right hand side of the simulated stylolite shows the actual dissolution and illustrate that dissolution is underestimated when the distance between the highest and lowest tip of the spikes on the stylolite are used to estimate compaction. The picture on the right hand side of figure 4b shows a stylolite with a geometry that is very similar to the simulation. This indicates that the noise in the natural example has a relatively constant scale and the grain size is probably relatively uniform which is underpinned by microscopic analysis not shown in this study. In general it can be stated that the numerical model can capture the complex geometries of natural stylolite examples. This implies that the model captures the main characteristics of stylolite growth and is realistic.

5.2. Bimodal noise, stylolite growth and compaction estimates

Figure 5 shows the progressive growth of a stylolite with pronounced teeth for three different time steps, after 2000, 4000 and 6000 model steps. These steps do not correspond to real time but are a function of the vertical strain and thus the compaction applied to the stylolite – these

corresponds to an average of xx, yy and zz dissolved particle rows. Large grains that pin the surface are shown in grey and the actual amount of host-rock dissolution is shown in grey bars on the right hand side of the three stylolites. Grains that pin the interface are initially relatively close to the starting dissolution surface so that pinning results already in pronounced teeth in the first time step shown (t=2000). Parts of these pinning grains survive and pin the surface until the last time step. This means that only initially a small part of the compaction is not recorded by the stylolite but at later stages the teeth record the full amount of dissolved host-rock. This will change once the pinning grains are dissolved themselves and pinning stops. During time steps 2000 and 4000 the stylolite geometry is still controlled by the large pinning grains on the one hand and by the small scale roughness that develops due to pinning on the particle scale. The latter results in the rough stylolite surface in the centre of the stylolite at time step 4000 where a number of wavelengths develop. At time step 6000 the geometry is mainly controlled by the large scale pinning grains since most of these meet with the stylolite interface. Each tip of a tooth contains small rests of these slower dissolving grains. Some of the teeth record almost the full compaction (from one side) because they met the stylolite relatively early and started to grow from the centre of the stylolite. Others, however, do not really record the full compaction since they either met the interface during a later stage of growth or they met an already developing tooth and are now dissolving the host-rock in the other direction. This can be seen for example at time step 2000, when a small grain on the left hand side of the stylolite meets the left corner of a tooth (see arrow in Fig. 5a). The grain is now “pushing” upwards into the host-rock, the developing tooth meets the original orientation of the interface during time step 4000 and moves upwards at time step 6000. One can use the distance between the highest and lowest tooth in such a stylolite to estimate compaction. Note that unless two slower dissolving grains are positioned next to each other but on opposite sides of the stylolite and pin the interface, each stylolite tooth will only record half of the compaction since they start out from one side of the stylolite (Fig. 5). In contrast to

311 the non-linear growth of stylolites that grow in more uniform rocks (Koehn et al., 2007 Ebner
312 et al. 2009a), a stylolite with a bimodal noise and strongly pinning grains grows linear with a
313 growth exponent of about 1.0. – up to the moment where slowly dissolving grains would meet
314 and destroy this large teeth growing in a ballistic (or fast) mode, to get more fluctuating peak
315 growth: a transition to a nonlinear growth similar to the more uniform rock type is then
316 expected.
317
318 *5.3. Stress scaling*
319 In the last set of simulations, we perform runs with a uniform noise and vary the stress on the
320 stylolite. We model stylolites that grew under a vertical stresses of 29, 41, 50, 57, 64, 71, 80
321 and 92 MPa. All stylolite simulations run for 8000 model time steps, each stress state is
322 modelled three times. We then analyze the roughness and try to recover the stress from the
323 stylolite morphology using the crossover length, where we average the results of the three
324 different runs per stress state. Examples of the finite stylolite pattern are shown in Figure 6,
325 where we present two stylolites for each stress state from 29 to 80 MPa. Variations in noise in
326 these cases are only a function of a different random seed of quenched noise i.e. the
327 heterogeneities in the system for each simulation.
328 Figure 6 illustrates the difficulty to see a relationship between the amount of stress that a
329 stylolite experienced and the stylolite roughness directly from the geometry of the roughness.
330 This is also illustrated by the variation in stylolite shape at constant stress depending only on
331 the random distribution of slowly dissolving particles (right versus left hand side in figure 6).
332 There may be a general trend from more wavy stylolites at lower stresses to more spiky
333 stylolites at higher stresses, but this relation is not clear. Therefore one has to use statistical
334 tools in order to analyze the stylolite roughness.
335 In order to determine the scaling of the interface roughness and cross-over length scale from
336 the simulated and natural stylolites we use the Fourier method (e.g. Barabasi & Stanley, 1995;

337 Schmittbuhl et al., 1995). We calculate the Fourier power spectrum *P(k)* i.e., the square of the
338 modulus of the Fourier transform, as a function of the wave-number *k* [1/lengthscale (mm^{-1})]
339 for each stylolite pattern. For the simulations we take averages of the power spectra of three
340 runs and plot the resulting average power spectrum as a function of *k* in log-log space. If the
341 roughness is self-affine the plot shows (Fig. 3) a linear slope, which is a function of the Hurst
342 exponent (Renard et al., 2004; Schmittbuhl et al., 2004)

343 $$P(k) \sim k^{-1-2\alpha}. \qquad (4)$$

344 Figure 7a shows the power spectrum as a function of the wave-number for the natural stylolite
345 of figure 1 and figure 7b an average of three numerical simulations. Both plots are similar,
346 with the natural data spanning over a wider range of magnitudes than the simulated data but
347 the simulated data having less noise in the signal because it is averaged over three runs. Since
348 the wave-number in the plots is a function of 1/wavelength, the left hand side of the plots
349 represents the larger wavelengths. Here the plots show two slopes, separated by a well-
350 defined crossover wavelength. These two self-affine regimes correspond to the elastic energy
351 dominated regime at the large scale and the surface energy dominated regime at the small
352 scale. On the very right hand side of the two plots the slope becomes flatter at a length scale
353 comparable to the particle size in the model and the drawn bitmap of the natural example.
354 This flat portion of the signal has to be cut off for the analysis of the cross-over length scale.
355 In order to fit a curve to the graphs we bin the data: it becomes clear in Figure 7c and d that in
356 the binned data set the two slopes become more visible. To avoid bias due to improper fitting
357 of the crossover-length that separates the two slopes we use a nonlinear least square curve-
358 fitting algorithm in logarithmic space (Ebner et al. 2009b) with predefined roughness
359 exponents of 1.1 and 0.5 for the surface energy and elastic dominated regimes, respectively
360 (Ebner et al., 2009b). The resulting cross-over *l* is then used for further analysis.
361 Figure 8 shows the result of the 24 simulations where the vertical stress component of the
362 simulated stylolites is plotted against the inverse of the square root of the cross-over

according to the scaling function of equation (2). The determined cross-over in the simulations is clearly a function of the stress on the stylolite and shows the right scaling relation:

$$\sigma_z = a\sqrt{1/l}\,, \qquad (5)$$

similarly to equation (2), since the boundary condition used in these simulations also correspond to a fixed vertical stress and fixed lateral displacement along x, as the one used to derive equation (2). The slope *(a)* of the linear regression line of the data is a function of the input parameters in equation (2) of the numerical model. The slope is almost identical with the input parameters of the numerical model (square root of Young's modulus times surface energy divided by κ), which shows that the scaling relation derived analytically and presented by Schmittbuhl et al. (2004) is verified by the numerical stylolite morphologies and is independently produced by the current numerical model presented here. This thus constitutes another completely independent check of this analytical expression, after the comparison of the overload stresses with the one determined from the crossover length for the stylolites investigated by Ebner et al. (2009b) in Southern France.

6. Methodology and application to natural cases

As an example for a paleo-stress calculation, we can use the natural stylolite shown in Figure 1 and the determined cross-over in Figure 7c. The calculation gives a vertical stress of about 34 MPa, a horizontal stress of about 13 MPa, a mean stress of 23.5 MPa and a differential stress of 21 MPa. If we assume that the overlying sediments in the basin had a density of about 2.5 kg/cm^3, the paleo-depth of the stylolite was about 1400 m in the basin. The orientation of the teeth or spikes of the stylolite indicates that the direction of the main compressive stress was vertical and that the stylolite formed in the sedimentary basin during burial. A limit with these calculations will always be the uncertainty in the input parameters

like the Young's Modulus, Poisson's ratio and the surface free energy at the time of stylolite formation. We used a relatively high Young's Modulus for the numerical simulations (80 GPa). The real limestone may have a lower value of about 50 GPa and this would change the stress and depth estimates (26.5 MPa vertical stress and 1100 m overburden). It is always advisable to use a range of natural stylolites for depth estimates as proposed in the work of Ebner et al. (2009b). In addition to the stress calculation, one can estimate the amount of dissolved material at the stylolite. According to the presented simulations the stylolite shown in figures 1 and 4b (right hand side) developed in a host-rock with a relatively uniform grain size. If the stylolite grew in a similar way than the simulations (Fig. 4b) then the dissolved material at the interface is in the order of 3 cm. However, since the grain size in the natural example is about $1/10^{th}$ of the size of the model particles, the actual amount of dissolved material at the interface is probably larger, because the amount of dissolved material depends on the grain size (equation 6). The scaling relation of Koehn et al. (2007)

$$A = b\left(\frac{w}{L}\right)^{1/0.8} L, \qquad (6)$$

where the prefactor b is 10 (factor varies, see Koehn et al., 2007 and Ebner et al., 2009a), A is the dissolved material (mm), w the mean RMS width of the interface in millimeter (for details of calculation compare Koehn et al., 2007 and Ebner et al., 2009a)and L the grain size (mm), with a grain size of about 0.01 mm for the natural example and a mean width of the interface of 2mm, results in an estimation of roughly 7.5 cm of material dissolved at the interface or 40 times the mean width of the interface. It is thus not possible to deduce the amount of dissolution directly from the finite interface morphology.

7. Conclusions

We modelled the development of stylolite patterns using a rock matrix that contains either a uniform or a bimodal grain size. Stylolites that developed from a bimodal noise show

pronounced teeth with straight edges and grow linearly with a growth exponent of about 1.0. The morphology produced by the simulations is similar to field observations. The distance between the maximum and minimun height of a tooth above and below the original dissolution surface can be used to estimate compaction if pinning starts relatively early during stylolite growth, and pinning grains are not completely destroyed during successive dissolution, thus giving a value that only slightly underestimates the true dissolution along the interface. Stylolites that develop in a rock that has a noise that sits on a uniform grain size may contain spikes but the height of these asperities highly underestimates compaction. For these stylolites the mean width of the interface should be calculated and the scaling law of Koehn et al. (2007) should be used to estimate compaction.

Modelling the growth of stylolites that developed under different normal stresses shows stylolite patterns that can be best distinguished using statistical methods. We use the Fourier method to extract the cross-over length scale from the numerical stylolites, calculate the predicted theoretical vertical stress values and compare them with the actual values used in the numerical simulations. The results are consistent and we can show that the numerical model reproduces the proposed scaling relation, thus our numerical model gives an independent confirmation of the analytical solution of Schmittbuhl et al. (2004). This analytical solution to determine paleo-stress magnitudes from stylolite shapes seems to be robust: the analytical result is verified for sets of stylolites obtained with two independent techniques, namely the ones produced with the current numerical model, and natural examples investigated by Ebner et al. (2009), whose burial stresses were inferred from their relative position in the stratigraphic column. To summarize, comparing numerical simulations with the stylolite shown on Figure 1b indicates that this stylolite formed during burial in a basin, at depth close to 1400 m, and accommodated about 7.5 cm of dissolution.

Acknowledgements

Koehn and Ebner acknowledge funding by the DFG (KO 2114/5). Toussaint and Renard acknowledge support of a FORPRO CNRS/ANDRA grant.

References

Aharonov, E., Katsman, R., 2009. Interaction between pressure solution and clays in stylolite development: insights from modeling. American Journal of Science 309, 7, 607-632.

Barabasi, A. L., Stanley, H. E., 1995. Fractal concepts in surface growth. Cambridge University Press.

Baron M., Parnell J., 1979. Relationships between stylolites and cementation in sandstone reservoirs: Examples from the North Sea, UK and East Greenland. Sedimentary Geology 194, 17-35.

Beach, A., 1979. Pressure solution as a metamorphic process in deformed terrigenous sedimentary rocks. Lithos 12, 51-58.

Bons, P. D., Koehn, D., Jessell, M. W., 2008. Microdynamics Simulation. In: Lecture Notes in Earth Sciences **106**. Springer, Berlin.

Brouste, A., Renard, F., Gratier, J. P., Schmittbuhl, J., 2007. Variety of stylolites' morphologies and statistical characterization of the amount of heterogeneities in the rock. Journal of Structural Geology 29, 422-434.

Burkhard M., 1993. Calcite twins, their geometry, appearance and significance as stress-strain markers and indicators of tectonic regime: a review. J. Struct. Geol. **15**, 3-5, 351-368.

Clark, S. P. J., 1966. Handbook of Physical Constants. Geological Society of America, New York.

Dunnington, H. V., 1954. Stylolite development post-dates rock induration. Journal of sedimentary Petrology 24, 27-49.

Ebner, M., Koehn, D., Toussaint, R., Renard, F., 2009a. The influence of rock heterogeneity on the scaling properties of simulated and natural stylolites. Journal of Structural Geology 31, 72-82.

Ebner, M., Koehn, D., Toussaint, R., Renard, F., Schmittbuhl, J., 2009b. Stress sensitivity of stylolite morphology. Earth and Planetary Science Letters 277, 394-398.

Ebner, M., Toussaint, R., Schmittbuhl, J., Koehn, D., Bons, P. 2010a. Anisotropic scaling of tectonic stylolites: a fossilized signature of the stress field? J. Geophys. Res. 115, B06403.

Ebner, M., Piazolo, S.,Renard, F., Koehn, D., 2010b. Stylolite interfaces and surrounding matrix material: Nature and role of heterogeneities in roughness and microstructural development. Journal of Structural Geology 32, 1070-1084.

Fabricius, I.L., Borre, M.K., 2007. Stylolites, porosity, depositional texture and silicates in chalk facies sediments. Ontong Java Plateau – Gorm and Tyra fields, North Sea. Sedimentology 54, 183-205.

Fletcher, R. C., Pollard, D. D., 1981. Anti-Crack Model for Pressure Solution Surfaces. Geology 9, 419-424.

Gratier, J. P., Muquet, L., Hassani, R., Renard, F., 2005. Experimental microstylolites in quartz and modeled application to natural stylolitic structures. Journal of Structural Geology 27, 89-100.

Guzzetta, G., 1984. Kinematics of Stylolite Formation and Physics of the Pressure-Solution Process. Tectonophysics 101, 383-394.

Heald, M. T., 1955. Stylolites in Sandstones. Journal of Geology 63, 101-114.

485 Katsman, R., Aharonov, E., Scher, H., 2006. A numerical study on localized volume
486 reduction in elastic media: some insights on the mechanics of anticracks, JGR, 111,
487 B3, B03204.
488 Karcz, Z. Scholz, C. H., 2003. The fractal geometry of some stylolites from the Calcare
489 Massiccio Formation, Italy. Journal of Structural Geology 25, 1301-1316.
490 Koehn, D., Arnold, J., Jamtveit, B., Malthe-Sørenssen, A., 2003. Instabilites in stress
491 corrosion and the transition to brittle failure. American Journal of Science 303, 956-
492 971.
493 Koehn, D., Malthe-Sørenssen, A., Passchier, C.W., 2006. The structure of reactive grain
494 boundaries under stress containing confined fluids. Journal of Chemical Geology 230,
495 207-219.
496 Koehn, D., Renard, F., Toussaint, R., Passchier, C. W., 2007. Growth of stylolite teeth
497 patterns depending on normal stress and finite compaction. Earth and Planetary
498 Science Letters 257, 582-595.
499 Lacombe, O., 2010. Calcite Twins, a Tool for Tectonic Studies in Thrust Belts and Stable
500 Orogenic Forelands, Oil & Gas Science and Technology – Rev. IFP Energies
501 nouvelles, 65, 809-838.
502 Merino, E., 1992. Self-organization in stylolites. American Scientist 80, 466.
503 Park, W. C., Schot, E. H., 1968. Stylolites: their nature and origin. Journal of sedimentary
504 Petrology 38, 175-191.
505 Petit, J. P., Mattauer, M., 1995. Paleostress Superimposition Deduced from Mesoscale
506 Structures in Limestone - the Matelles Exposure, Languedoc, France. Journal of
507 Structural Geology 17, 245-256.
508 Railsback, L. B., 1993. Lithologic Controls on Morphology of Pressure-Dissolution Surfaces
509 (Stylolites and Dissolution Seams) in Paleozoic Carbonate Rocks from the Mideastern
510 United-States. Journal of Sedimentary Petrology 63, 513-522.
511 Renard, F., Schmittbuhl, J., Gratier, J. P., Meakin, P., Merino, E., 2004. Three-dimensional
512 roughness of stylolites in limestones. Journal of Geophysical Research-Solid Earth
513 109 (B3).
514 Rispoli, R., 1981. Stress-Fields About Strike-Slip Faults Inferred from Stylolites and Tension
515 Gashes. Tectonophysics 75, T29-T36.
516 Rutter, E. H., 1983. Pressure solution in nature, theory and experiment. Journal of the
517 Geological Society of London 140, 725-740.
518 Schmittbuhl, J., Vilotte, J. P., Roux, S., 1995. Reliability of Self-Affine Measurements.
519 Physical Review E 51, 131-147.
520 Schmittbuhl, J., Renard, F., Gratier, J. P., Toussaint, R., 2004. Roughness of stylolites:
521 Implications of 3D high resolution topography measurements. Physical Review
522 Letters 93, 238501.
523 Tada, R., Siever, R., 1989. Pressure Solution during Diagenesis. Annual Review of Earth and
524 Planetary Sciences 17, 89-118.
525

526 Figure captions

527 Figure 1: Example of the same natural stylolite in limestone, at different scales. On the large

528 scale, the stylolite is relatively flat whereas the aspect ratio of the roughness (out-of-plane

529 dimension over in-plane one) increases towards smaller scales from a to c. Between c and d

530 the roughness aspect ratio remains constant.

Figure 2: a) Sketch showing typical stylolite teeth where the sides of the teeth are oriented parallel to the main compressive stress. In the example on the right hand side the teeth are inclined indicating that the main stylolite plane is oriented at an angle to the smallest principle stress σ_3. b) Sketch illustrating how stylolite teeth shown in a) can grow if impurities (dark cirlces) pin the interface. c) Sketch after Ebner et al. (2010b) showing how low solubility quartz grains may pin the sides of teeth in natural stylolites.

Figure 3: Model setups for the numerical simulations of stylolite roughening. The sidewalls are confined and the upper and lower walls are pushed inwards. Dissolution takes place along an initially flat line in the centre of the model. Dark particles dissolve slower. a) Setup for a uniform grain size where the particles in the model may represent grains in the rock. b) Setup for a bimodal grain size, where the small grains are represented by particles in the model whereas the large grains are defined by clusters of particles.

Figure 4: Results of the numerical simulations of stylolite roughening for a) a bimodal grain size and b) a uniform grain size. The actual dissolution of the host rock is indicated with grey vertical bars next to the stylolites. On the right hand side two natural stylolites are shown that may represent similar variations in noise than in the simulations. The grey patches along the stylolite indicate the largest grains that dissolve slower and act as pinning sites for the interface. Note the strong similarity between the numerical simulations and the natural stylolites.

Figure 5: Time sequence of simulated stylolite growth in a host rock with a bimodal grain size. Note that model steps are proportional to strain increments and amounts of dissolved material and not real time. Bars on the right hand side record the real amount of dissolved

material in the simulations. Note how largest grains (grey patches) pin the interface and produce pronounced teeth that record accurately the actual compaction.

Figure 6: Two sets of 7 stylolites that developed under increasing normal stress. Right and left hand stylolites only differ in initial random seeds of the quenched noise in the simulations. The relationship between the rough geometries and stresses cannot be visualized, even though there may be an increase in spikes from low to high stresses.

Figure 7: Fourier analysis of the roughness of stylolites, where the Fourier power spectrum *(P(k))* is plotted against the wave-number *(k)*, the inverse of the wavelength of the roughness. a) shows a Fourier analysis of a the natural stylolite shown in figure 1, b) an average of the Fourier analysis of 3 numerical stylolites. c) and d) show binned data sets of the Fourier power spectra of a) and b) and the presence of a well-defined crossover length scale.

Figure 8: Plot of the square root of the inverse of the determined crossover length from the numerical simulations against the applied stress following the scaling law of Schmittbuhl et al., (2004). The data plots roughly on a line illustrating that the simulations reproduce the scaling relation. Error bars represent variations in different cross-over length scales found in different simulations.

***Highlights**

Stylolites are stress gauges

Stylolites can be used to estimate compaction

Grain size distribution influences stylolite teeth growth

Stylolites with large pinning fossils grow linear

Stylolites with uniform grain size grow non-linear

Figure
Click here to download high resolution image

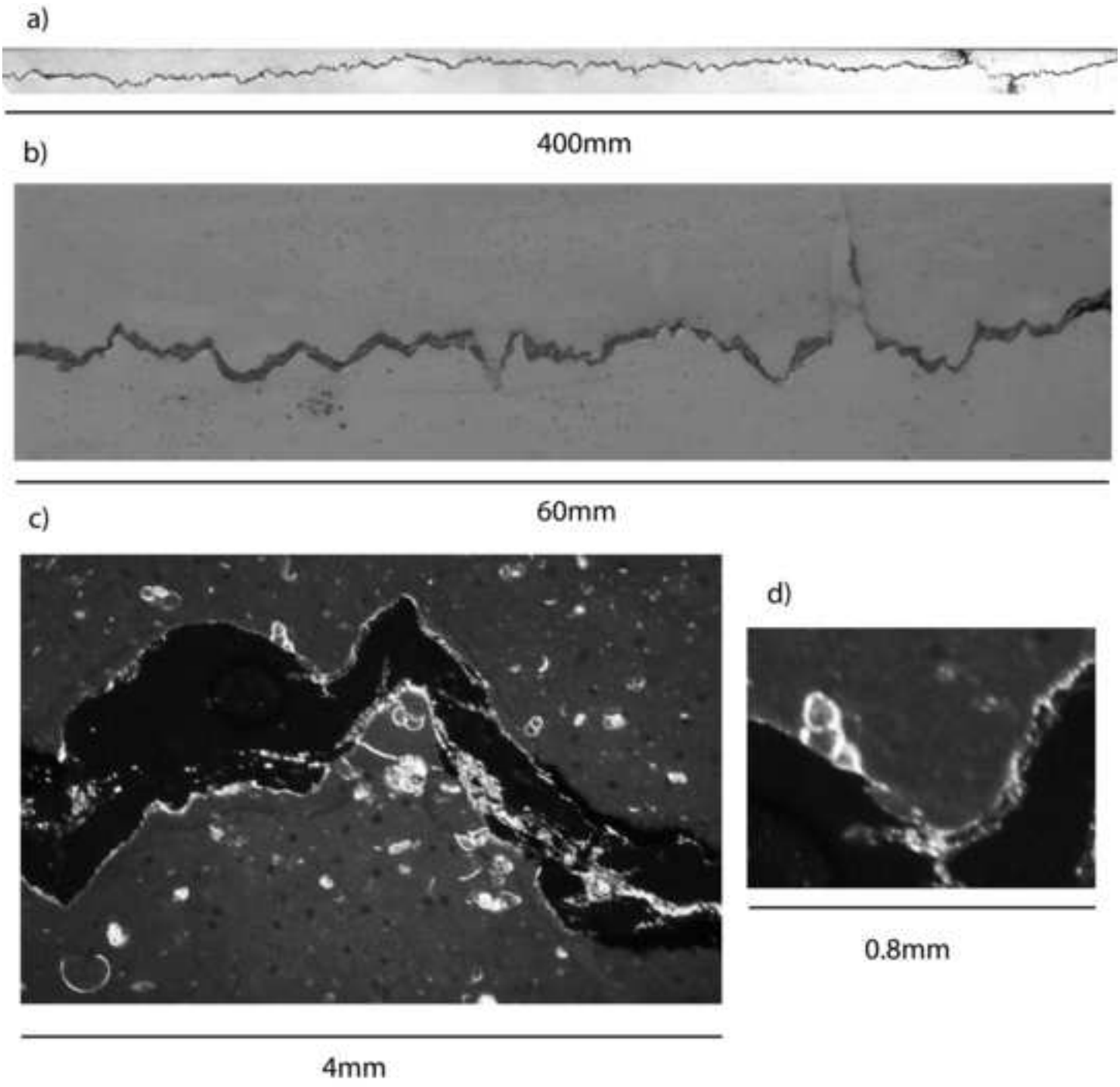

Fig. 1

Figure
Click here to download high resolution image

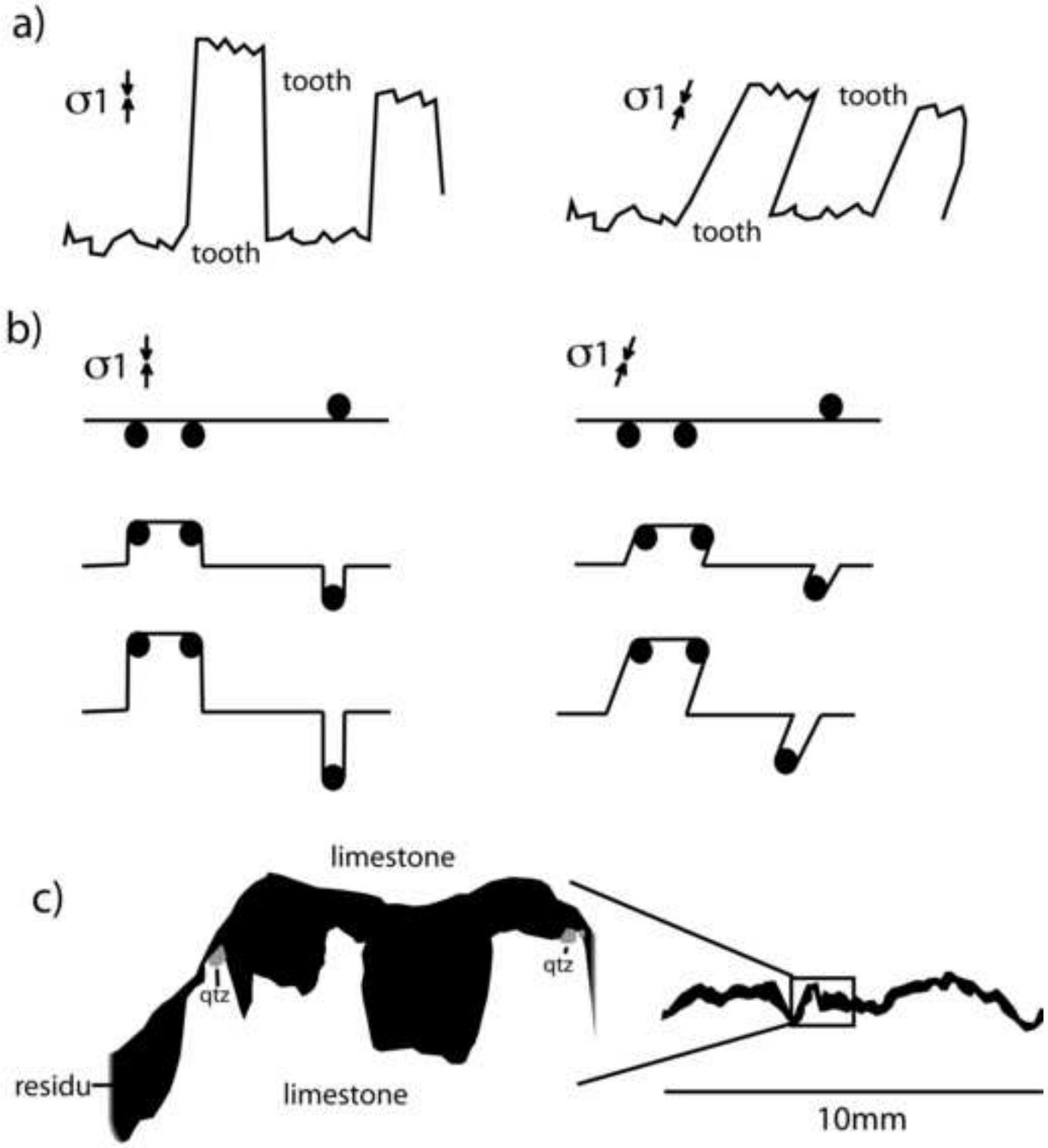

figure 2

Figure
Click here to download high resolution image

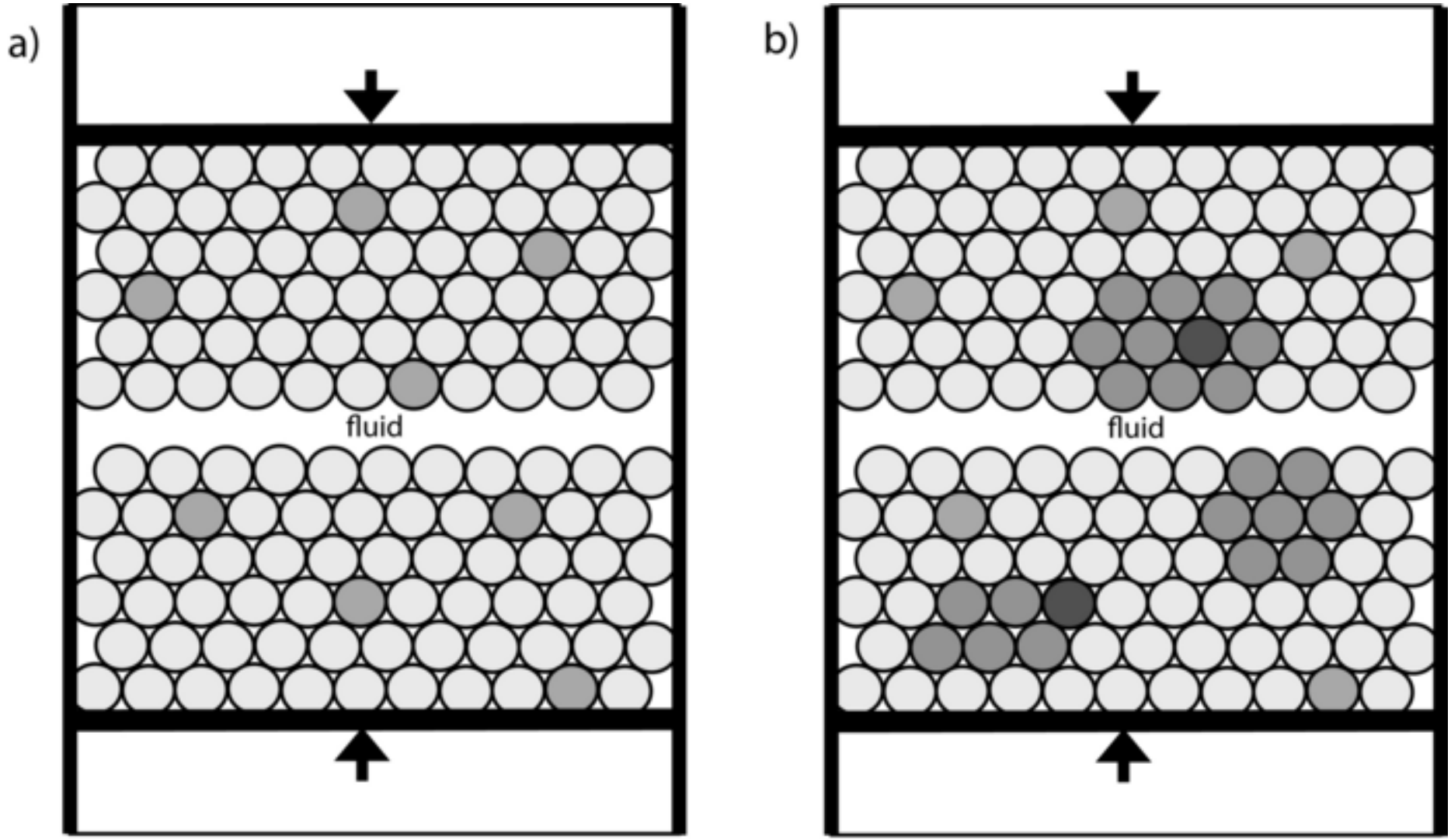

Figure 3

Figure
Click here to download high resolution image

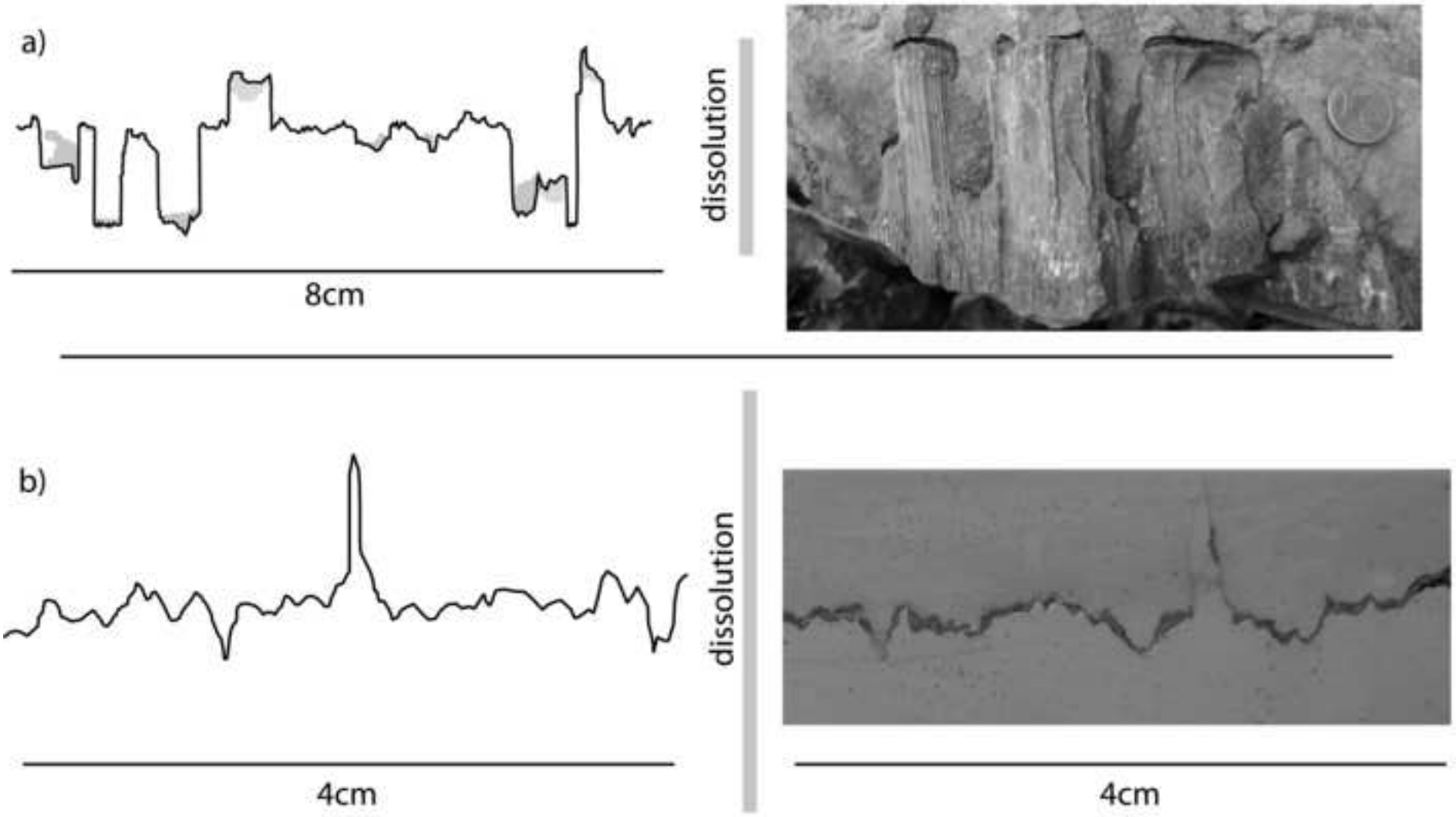

figure 4

Figure
Click here to download high resolution image

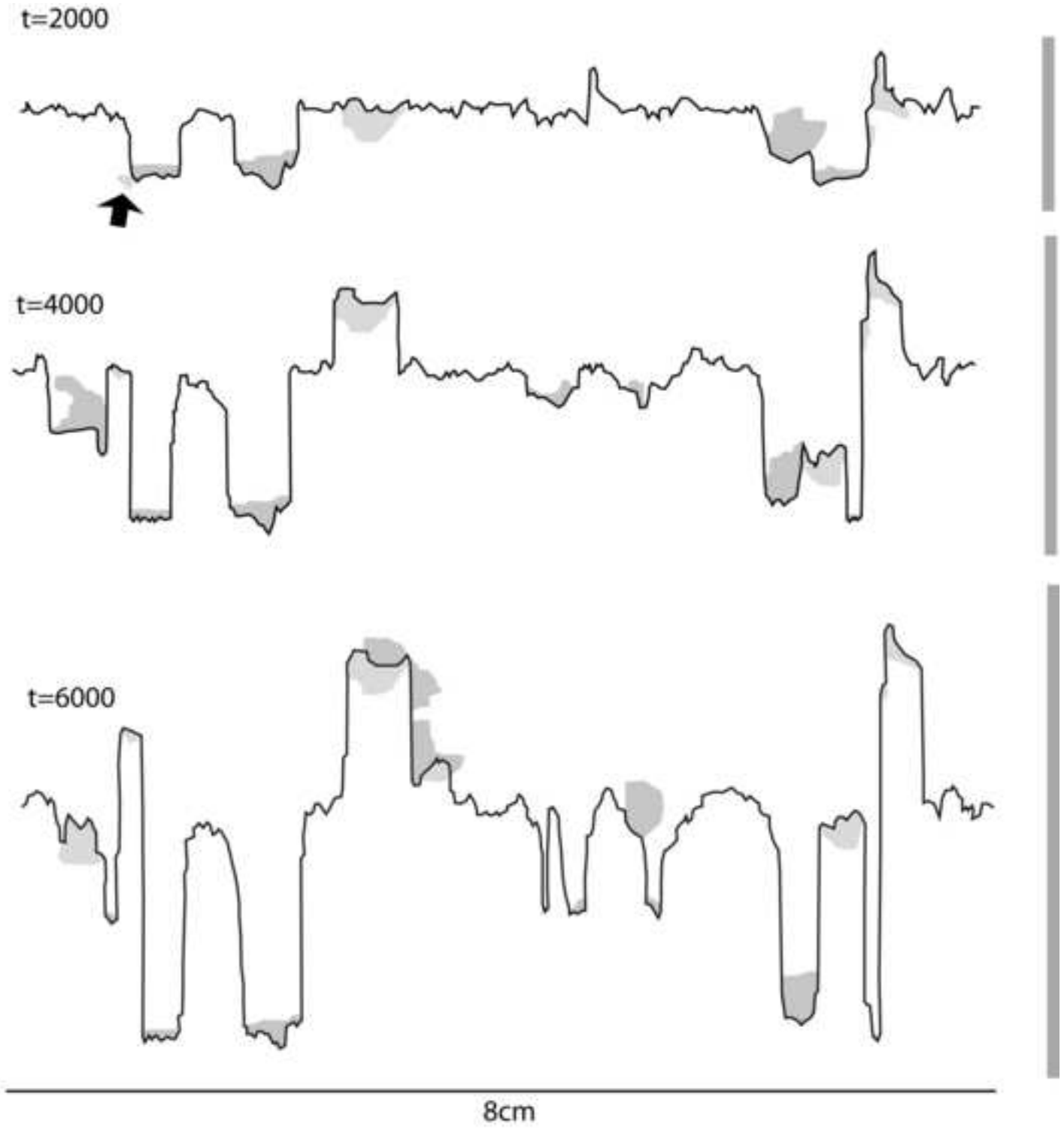

figure 5

Figure
Click here to download high resolution image

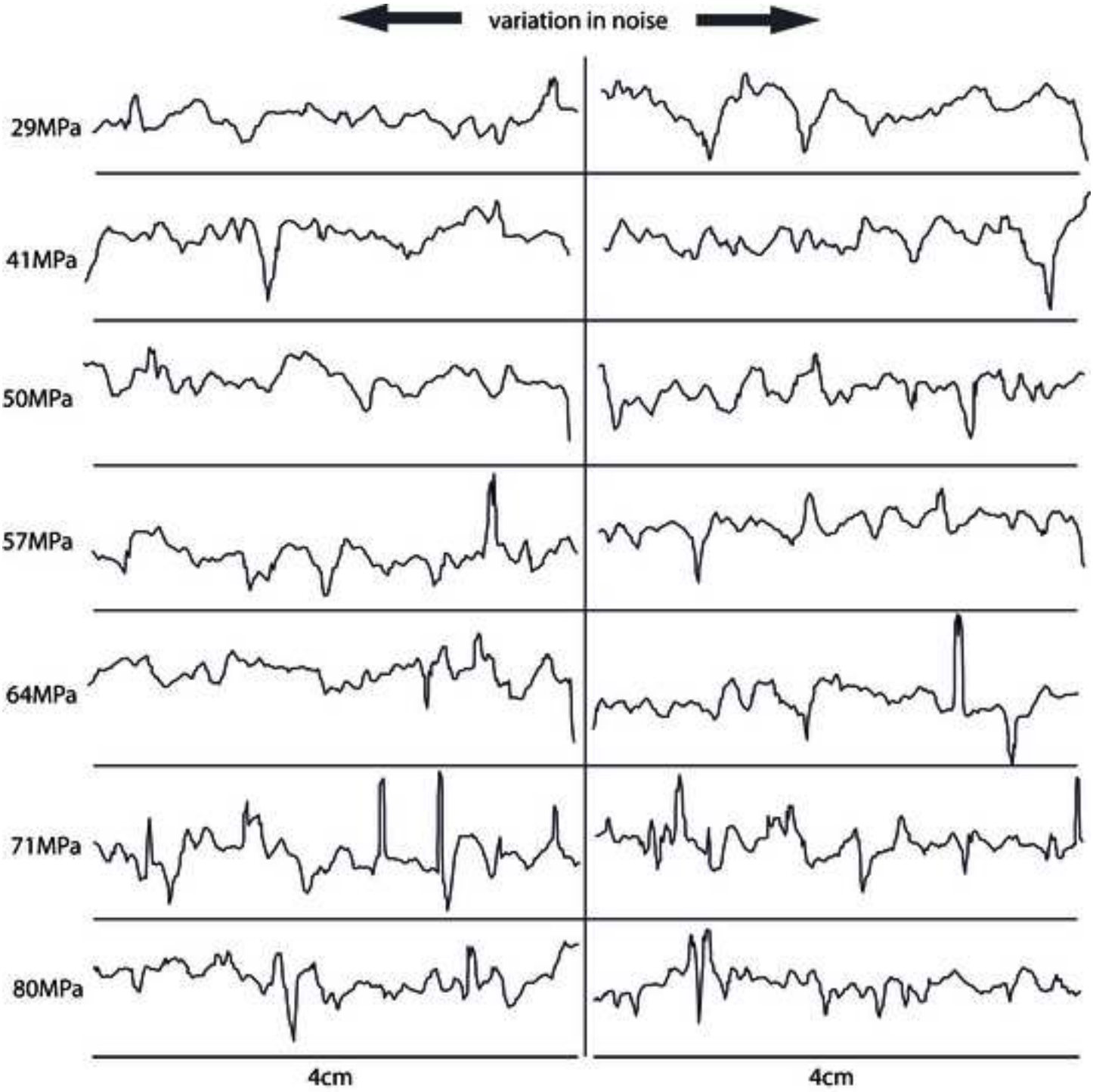

figure 6

Figure

Click here to download high resolution image

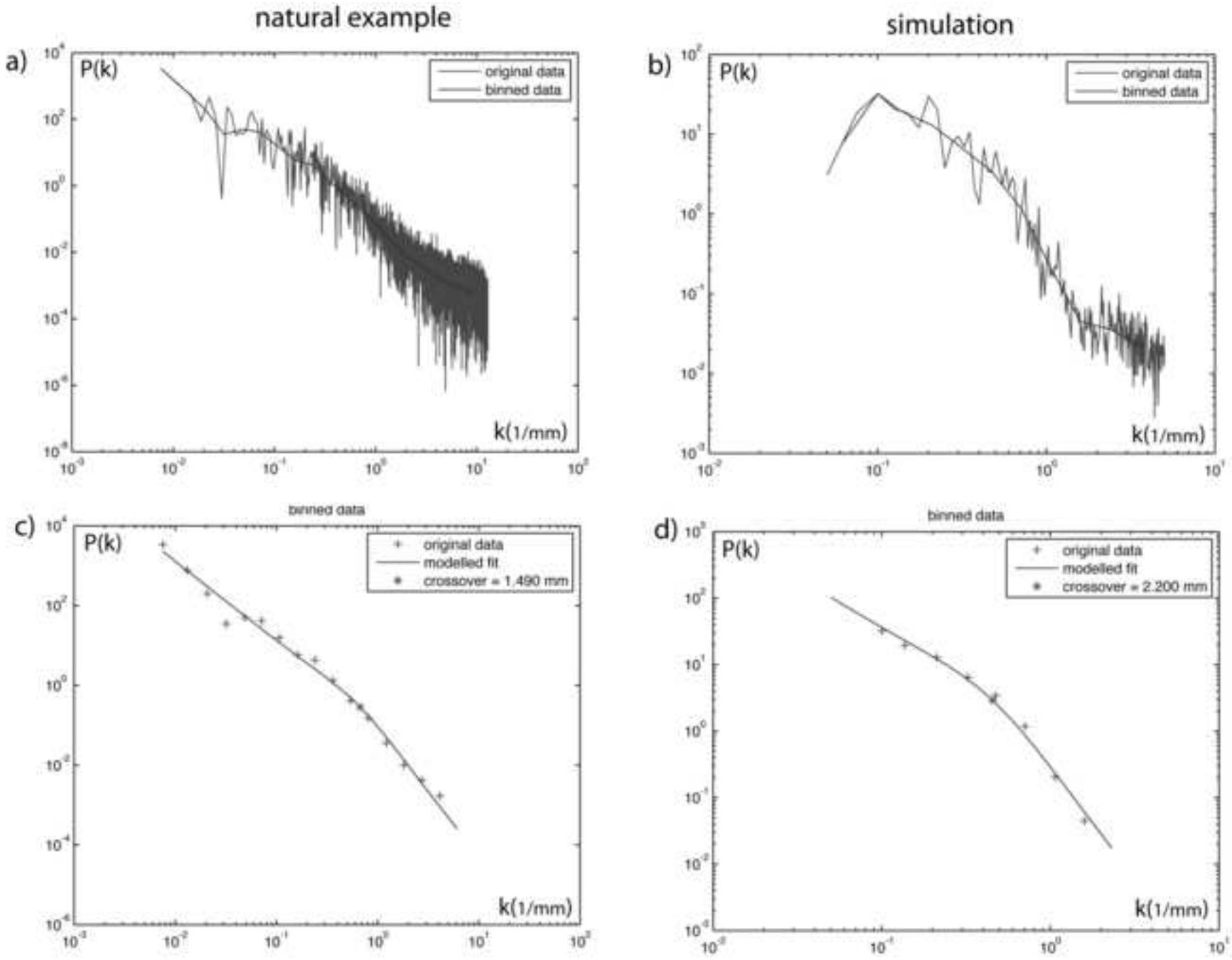

figure 7

Figure
Click here to download high resolution image

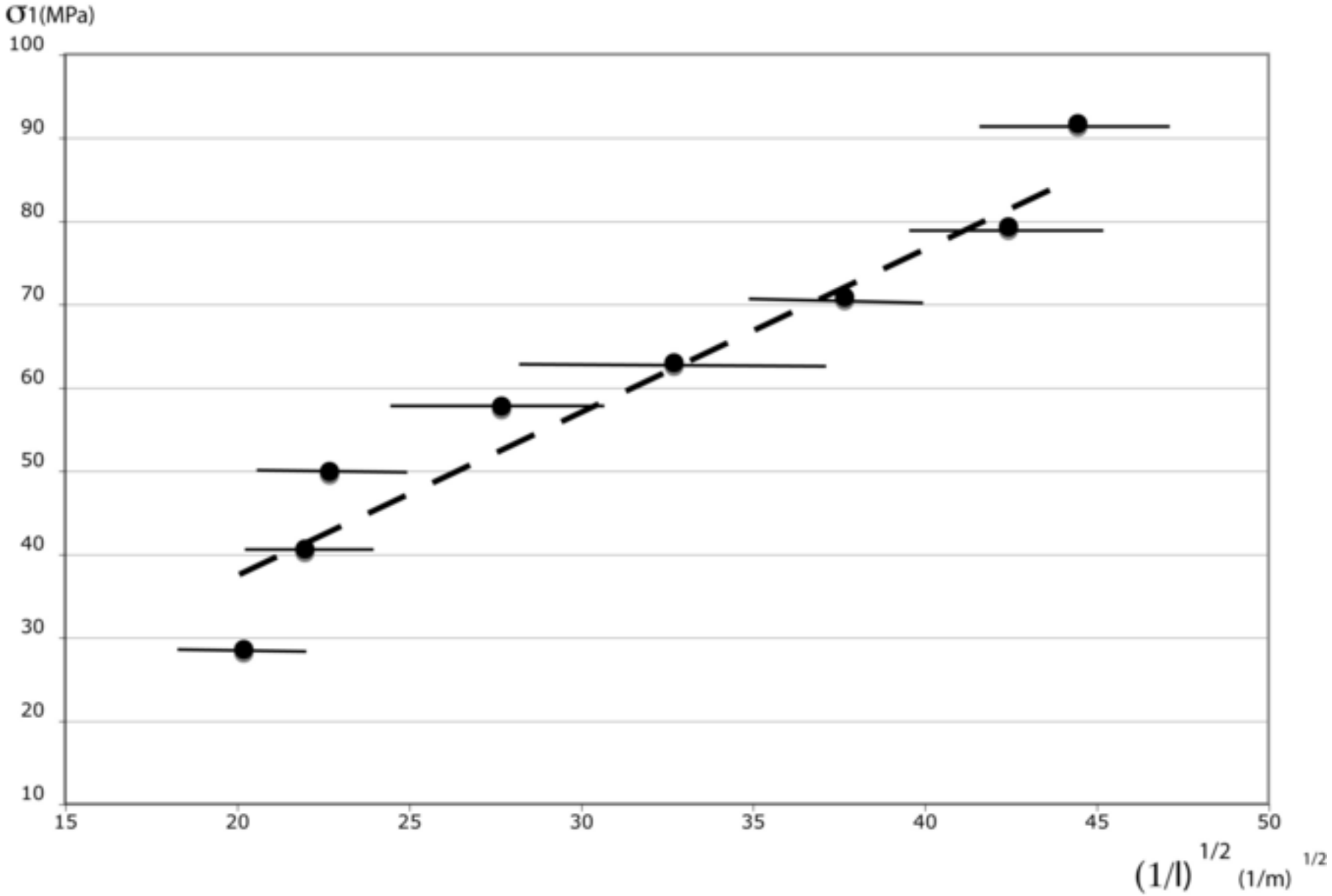

figure 8